ACS OMEGA

http://pubs.acs.org/journal/acsodf

Article

Sb_2TeSe_2 Monolayers: Promising 2D Semiconductors for Highly Efficient Excitonic Solar Cells

Chun Wang, Yu Jing, Xiaocheng Zhou,* and Ya-fei Li*

Cite This: *ACS Omega* 2021, 6, 20590−20597

Read Online

ACCESS | Metrics & More | Article Recommendations | Supporting Information

ABSTRACT: On the basis of density functional theory computations, we demonstrated that two-dimensional (2D) α- and β-Sb2TeSe2 monolayers are promising candidates for constructing high-efficiency heterojunction excitonic solar cells. These two 2D materials possess moderate band gaps (~1.1 eV), which can be flexibly tuned by applying external strains. They possess high carrier mobility (~3000 $cm^2 V^{-1} s^{-1}$) and can absorb sunlight over the whole range of the solar spectrum. Remarkably, the α- and β-Sb2TeSe2 monolayers can form desirable type II heterostructures with HfSe2 and BiOI monolayers, respectively. The power conversion efficiencies of α-Sb_2TeSe_2/$HfSe_2$ and β-Sb_2TeSe_2/BiOI heterojunction excitonic solar cells can reach 22.5 and 20.3%, respectively. Since α-Sb2TeSe2 and β-Sb2TeSe2 monolayers have good stability and high synthesis feasibility, they have important applications in photovoltaic solar cell devices.

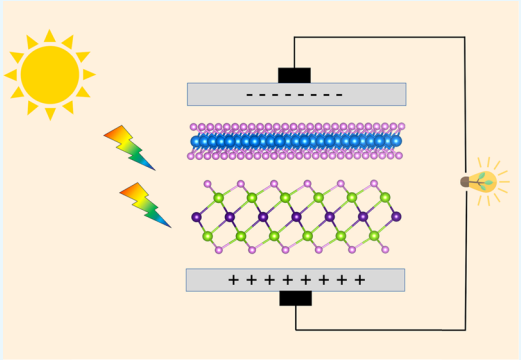

INTRODUCTION

Solar cell, which converts solar radiation directly into electricity, is an important and renewable energy-conversion technology. Since the development of the first practical solar cell in 1954,[1] solar cell materials with improved power conversion efficiency (PCE) have been explored continuously.[2−8] According to the photoelectric conversion mechanism, solar cells can be divided into two main categories, namely, conventional solar cells[2−4] and excitonic solar cells (XSCs).[5−8] The former consists of bulk inorganic semiconductors such as Si,[2] GaAs,[3] and CdTe,[4] in which the electron−hole pairs are directly generated in bulk materials. However, the production of traditional solar cell devices is a complex process requiring high energy consumption and causing serious environmental pollution. The latter category is composed of a heterostructure formed by two different materials or phases, including organic solar cells (OSCs),[5] dye-sensitized solar cells (DSSCs),[6] and two-dimensional (2D) heterojunction solar cells.[7,8] These XSCs usually have a high PCE, in which the light-induced excitons are generated and dissociated simultaneously at the donor−acceptor interface. Compared to other XSCs, 2D heterojunction solar cells are more promising for high-efficiency solar cell applications because of their superior interfacial effect. Meanwhile, 2D materials can form high-quality heterogeneous interfaces because of the absence of dangling bonds, promoting the research of vertical heterostructures. Moreover, many 2D materials possess exotic electronic and optoelectronic properties, making them attractive donor and acceptor materials for designing high-efficiency solar cells.[9]

In principle, 2D heterojunction solar cells with a high PCE should satisfy two main criteria.[8] First, 2D acceptor and donor materials can be assembled into a van der Waals (vdW) heterostructure with a type II band alignment. Second, the band gap of the donor material should be in the region of 0.90−1.70 eV to guarantee good light-harvesting performance. More precisely, the conduction band offset between the acceptor and donor materials should be within 0.20 eV. Although previous studies have proved that 2D XSCs can enhance the separation efficiency of photogenerated excitons at the interfaces and improve the photoelectric conversion performance, most 2D XSCs still exhibit a PCE of less than 20%.[10−12] The inherent reason is that in addition to the separation efficiency of excitons, the carrier mobility and the light-harvesting performance also play important roles in determining the PCE. Thus, searching for suitable 2D donor and acceptor materials with high carrier mobility and good light-harvesting performance is significant for the development of XSCs.

In this work, by means of density functional theory (DFT) computations, we designed two new 2D structures, named α- and β-Sb2TeSe2 monolayers, as promising candidates for 2D XSCs. Bulk α- and β-Sb_2TeSe_2[13] with layered configurations

Received: May 26, 2021
Accepted: July 13, 2021
Published: July 27, 2021

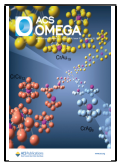

are topological materials and have been widely investigated in recent years.[13−15] Our computations have revealed that the α- and β-Sb_2TeSe_2 monolayers show good dynamical and thermal stability and can be easily exfoliated from the bulk phases due to the weak interlayer interaction. Furthermore, both the α- and β-Sb_2TeSe_2 monolayers are semiconductors with a band gap of ∼1.1 eV and exhibit high carrier mobility of ∼3000 $cm^2 V^{-1} s^{-1}$, suggesting that they could serve as promising donor materials to construct efficient 2D heterojunction XSCs. We further demonstrated that the 2D XSCs based on α-Sb_2TeSe_2/$HfSe_2$ and β-Sb_2TeSe_2/BiOI heterojunctions can exhibit ultrahigh PCEs of 22.5 and 20.3%, respectively.

COMPUTATIONAL METHODS

All DFT calculations were performed using the Vienna ab initio simulation package (VASP).[16] The projector-augmented-wave (PAW) approach was applied to describe the electron−ion interactions.[17,18] The Perdew−Burke−Ernzerhof (PBE) functional[19] within the generalized gradient approximation (GGA) was chosen for structural optimizations, while the Heyd−Scuseria−Ernzerhof (HSE06) hybrid functional[20] was employed for more accurate calculations of electronic properties. The spin−orbital coupling (SOC) effect[21] was also taken into account in the band structure computations due to the existence of heavy elements in the Sb2TeSe2 monolayers. We adopted a vacuum space of at least 15 Å in the z-direction to avert interactions between adjacent layers, and the DFT-D3 (D stands for dispersion) method was used to correct van der Waals (vdW) interactions.[22] A 500 eV cutoff for the plane-wave expansion was adopted in all of the computations. The convergence criteria were set as 10^{-5} eV for the energy and 0.01 eV $Å^{-1}$ for the force. The 2D Brillouin zone was sampled by a Monkhorst−Pack k-point mesh of 9 × 9 × 1 and 13 × 13 × 1 for geometry optimizations and electronic structure computations, respectively. The phonon band structures of the α/β-Sb2TeSe2 monolayers were computed using the density functional perturbation theory (DFPT)[23] as implemented in the PHONOPY package.[24] The first-principles molecular dynamics (FPMD) simulations were performed to evaluate the thermal stability of the Sb_2TeSe_2 monolayers. The constant volume−constant temperature ensemble (NVT) was adopted.[25] The FPMD simulations lasted for 10 ps with a time step of 1.0 fs at 600 K. The temperature was controlled using the Nosé−Hoover method,[26] which controls the energy fluctuations of a thermostat variable by coupling it with another thermostat variable.

RESULTS AND DISCUSSION

Structural Properties and Stability of the Sb_2TeSe_2 Monolayers. Both α- and β-Sb_2TeSe_2 bulks are layered materials that crystallize in the hexagonal structures with the space groups $R\bar{3}m$ (No. 166) and $R3m$ (No. 160), respectively. In α- and β-Sb_2TeSe_2 bulks, the monolayers are stacked together with interlayer vdW interactions along the z-axis in an ABC sequence. Optimized at the PBE-D3 level of theory, the equilibrium lattice parameters of the α- and β-Sb_2TeSe_2 bulks are $a = b = 4.15$ Å, $c = 28.97$ Å and $a = b = 4.15$ Å, $c = 29.21$ Å, respectively, which are in good agreements with the experimental measurements.[13] Moreover, our computations demonstrated that both α-Sb_2TeSe_2 and β-Sb_2TeSe_2 bulks are semiconductors with band gaps of 0.57 and 0.54 eV, respectively, which are consistent with the previous theoretical studies.[27] However, the relatively small band gaps limit the applications of bulk α/β-Sb_2TeSe_2 for solar cell devices.

The α- and β-Sb_2TeSe_2 monolayers can be initially obtained by isolating individual layers from the bulks. As shown in Figure 1, both the α- and β-Sb_2TeSe_2 monolayers consist of

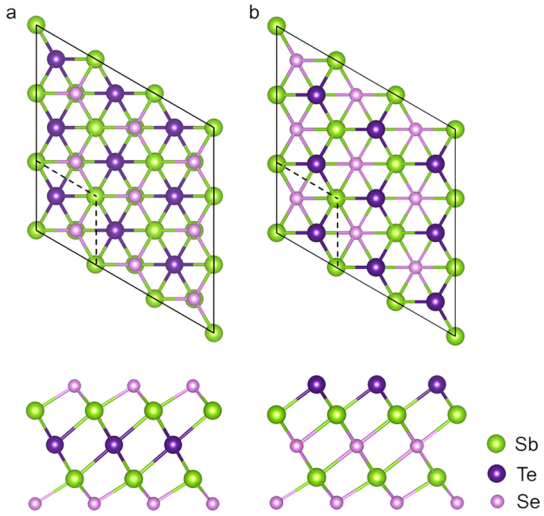

Figure 1. Top and side views of (a) α-Sb_2TeSe_2 and (b) β-Sb_2TeSe_2 monolayers. Pink, purple, and green balls represent Se, Te, and Sb atoms, respectively.

five close-packed atomic layers in the sequence of Se-Sb-Te-Sb-Se and Te-Sb-Se-Sb-Se, respectively. The optimized lattice parameters of the α-Sb_2TeSe_2 ($a = b = 4.13$ Å) and β-Sb_2TeSe_2 ($a = b = 4.13$ Å) monolayers are quite close to their bulk crystals.[27] The thicknesses of the α- and β-Sb_2TeSe_2 monolayers are 7.14 and 7.01 Å, respectively.

Experimentally, many 2D materials with weak interlayer interaction can be produced from their bulk materials via mechanical exfoliation.[27−30] We evaluated the experimental synthesis feasibility of the α- and β-Sb_2TeSe_2 monolayers by computing their cleavage energy (E_{cl}), which is defined as the minimum energy required to isolate a monolayer structure from the bulk. Specifically, the exfoliation processes for both α- and β-Sb_2TeSe_2 were simulated by imposing a fracture in a five-layer slab model, in which only the top layer is removable while the rest four layers are fixed. The E_{cl} of the α- and β-Sb_2TeSe_2 monolayers were then computed by increasing the separation distance between the two components. As shown in Figure 2a,c, the E_{cl} of the α- and β-Sb_2TeSe_2 monolayers first increases as the separation distance increases and then gradually converges to a constant value of 0.35 J m^{-2} when the separation distance is larger than 7 Å. Remarkably, the computed E_{cl} of the α- and β-Sb_2TeSe_2 monolayers are close to that of some 2D crystals that have been realized experimentally via exfoliation techniques, such as graphite (0.30 J m^{-2})[31] and MoS_2 (0.42 J m^{-2}),[32] suggesting the high feasibility of exfoliating 2D α- and β-Sb_2TeSe_2 monolayers from their bulk phases.

After evaluating the experimental feasibility, it is necessary to confirm the stability of the α- and β-Sb_2TeSe_2 monolayers, which is a prerequisite for their practical applications. We first accessed the dynamical stability of α- and β-Sb_2TeSe_2 monolayers by calculating the phonon dispersion curves. As shown in Figure 2b,d, all of the phonon modes are real and present in a typical form of 2D structures (one parabolic and

https://doi.org/10.1021/acsomega.1c02746
ACS Omega 2021, 6, 20590−20597

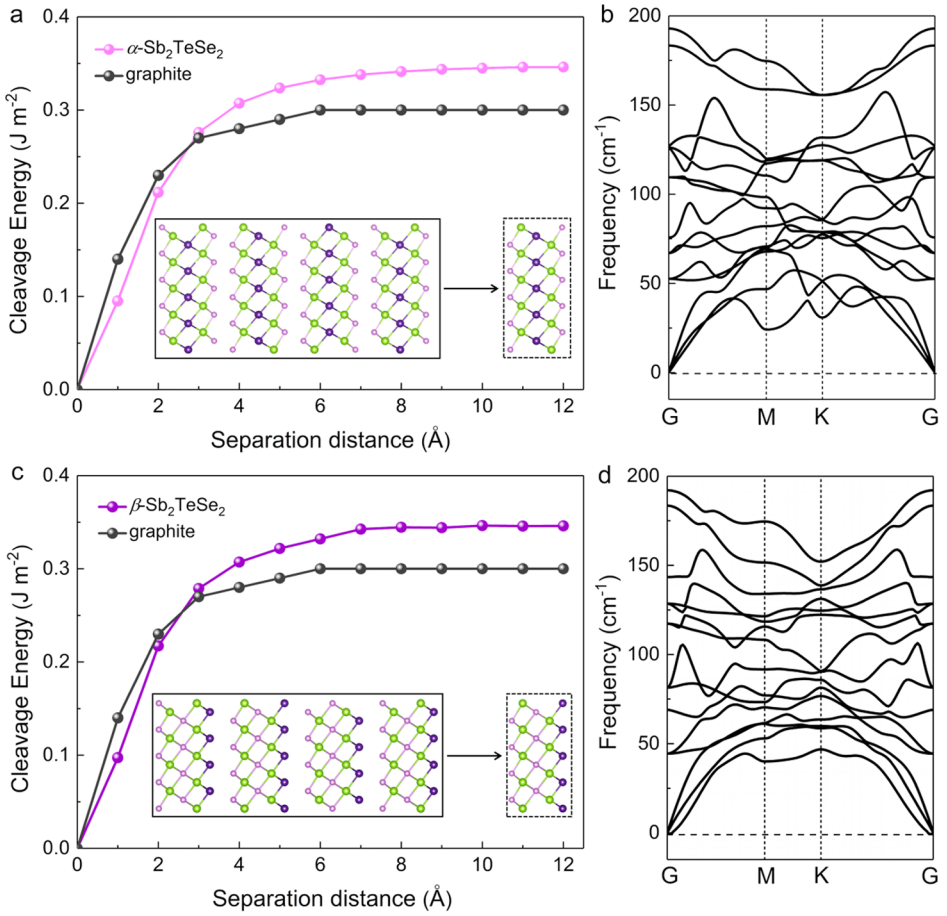

Figure 2. Cleavage energy E_{cl} as a function of the separation distance d for a fracture in (a) α- and (c) β-Sb_2TeSe_2 slabs in comparison with graphite. The inset is the schematic of separating a monolayer from its neighboring layers. The distance of zero corresponds to the equilibrium geometry. Phonon dispersion curves of (b) α- and (d) β-Sb_2TeSe_2 monolayers.

two linear acoustic branches starting from the G point), suggesting that 2D α- and β-Sb_2TeSe_2 monolayers are dynamically stable. We also carried out the FPMD simulations to assess the thermal stability of the α- and β-Sb_2TeSe_2 monolayers. To effectively avoid the confinement of periodic boundary conditions, a 5 × 5 supercell consisting of 125 atoms was adopted for both monolayers in the FPMD simulations. As shown in Figure S1, the α- and β-Sb_2TeSe_2 monolayers can maintain the structural integrity throughout a 10 ps FPMD simulation at a temperature of 600 K. Especially, the final structures can recover to the initial configurations after a full atomic relaxation, indicating the high thermodynamic stability of 2D α- and β-Sb_2TeSe_2 monolayers. The elastic constants (C_{ij}) of the α- and β-Sb_2TeSe_2 monolayers were also computed to evaluate the mechanical stability. By fitting the energy−strain curves, the elastic constants of the α- and β-Sb_2TeSe_2 monolayers were derived to be C_{11} = 64.31 N m^{-1}, C_{12} = 19.21 N m^{-1}, C_{66} = 22.56 N m^{-1} and C_{11} = 69.00 N m^{-1}, C_{12} = 17.56 N m^{-1}, C_{66} = 25.51 N m^{-1}, respectively, which meet well with the Born−Huang mechanical stability criteria for a rhombus 2D sheet ($C_{11} > |C_{12}|$, $C_{66} > 0$), suggesting the mechanical stability of the α- and β-Sb_2TeSe_2 monolayers.[33] Moreover, the work functions of α-Sb_2TeSe_2 (5.72 eV) and β-Sb_2TeSe_2 (5.44 eV) monolayer are much higher than those of graphene (4.60 eV) computed at the same PBE level, indicating that the α- and β-Sb_2TeSe_2 monolayers possess rather good chemical stability.

Electronic Properties of the Sb_2TeSe_2 Monolayers. We next systematically investigated their electronic properties by computing the electronic band structure and density of states (DOSs). Computed at the HSE06 level of theory, both the α- and β-Sb_2TeSe_2 monolayers are semiconductors with indirect band gaps of 1.17 and 1.09 eV, respectively. Especially, when the SOC effect was taken into account, the band gaps of the α- and β-Sb_2TeSe_2 monolayers decrease to 0.99 and 0.90 eV, respectively. As shown in Figure 3a,c, the reduction of the band gap is mainly caused by the downward shift in the conduction bands. A detailed analysis of the partial DOS (PDOS) reveals that the conduction band minima (CBMs) of the α- and β-Sb_2TeSe_2 monolayers are predominantly from the Sb 5p orbitals, while the valence band maxima (VBMs) are mainly derived from the Te 5p and Se 4p orbitals. Furthermore, we also visualized the partial charge density associated with the VBM and CBM for α- and β-Sb_2TeSe_2 monolayers. As shown in Figure 3b,d, the charge densities of CBM are mainly localized on the Sb atoms, while those of VBM are distributed around Te and Se atoms, which are in excellent agreement with the PDOS analysis. The above results imply that the photogenerated electron−hole pairs in the α- and β-Sb_2TeSe_2 monolayers could be effectively separated, which would facilitate their applications in optoelectronics.

Previous studies have proved that applying an external strain can effectively modulate the electronic properties of 2D structures.[34,35] Therefore, we also investigated the effect of the

https://doi.org/10.1021/acsomega.1c02746
ACS Omega 2021, 6, 20590−20597

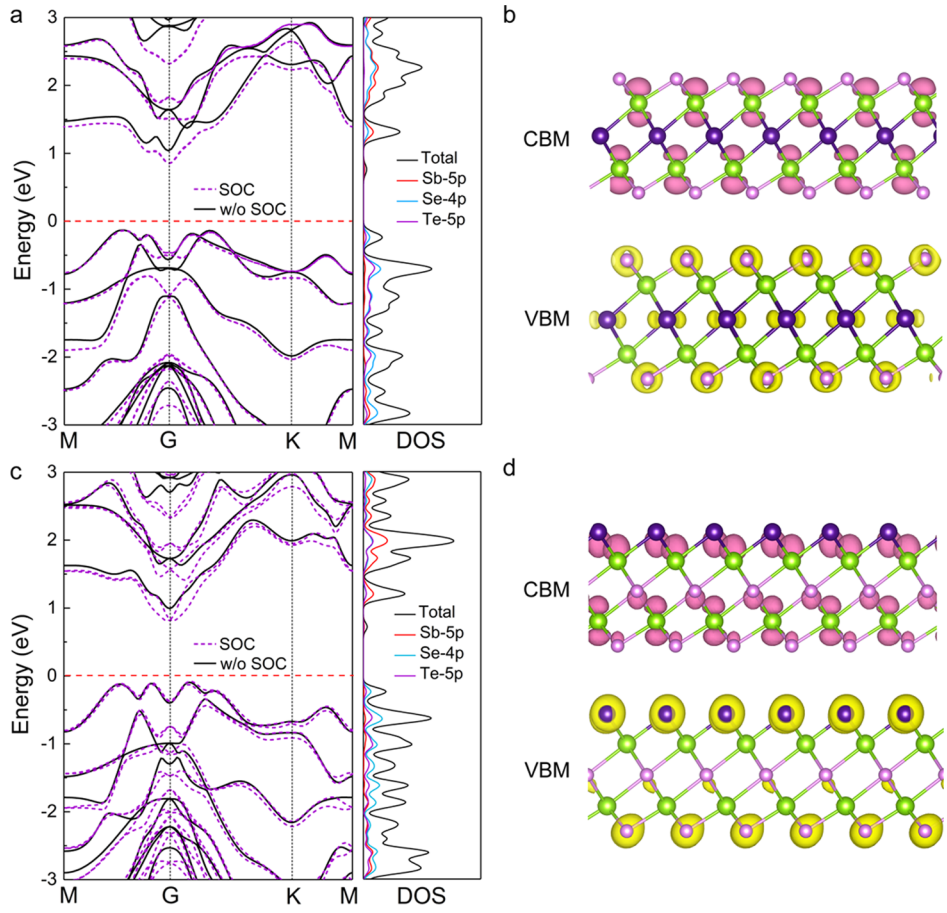

Figure 3. Electronic band structures and projected density of states of (a) α- and (c) β-Sb_2TeSe_2 monolayers calculated at the HSE and HSE + SOC level. Partial charge densities of (b) α- and (d) β-Sb_2TeSe_2 monolayers are indicated in pink for CBM and yellow for VBM. The isosurface value is 0.007 e $Å^{-3}$.

biaxial strain on the electronic properties of the α- and β-Sb_2TeSe_2 monolayers with the HSE06 method. Here, the strain (ε) is defined as $\varepsilon = (l - l_0)/l_0$, where l and l_0 are the strained and the equilibrium lattice parameters, respectively. Our computations demonstrated that applying an external strain can effectively tune the electronic structures of the α- and β-Sb_2TeSe_2 monolayers. As shown in Figure S2, when subjected to a tensile strain, the energy positions of the CBM for two monolayers are shifted downward faster than those of the VBM, leading to a decreased band gap with increased strain (Figure 4). Under a biaxial tensile strain of 6%, the band gaps of α- and β-Sb_2TeSe_2 monolayers are significantly reduced to 0.74 and 0.85 eV, respectively. In contrast to the tensile strain, applying a compression strain increases the band gaps as the energy positions of CBM for two monolayers are shifted upward faster than those of VBM. However, for the α-Sb_2TeSe_2 monolayer, there is a sudden drop in band gap when the compressive strain reaches −6%. This is because at this moment the location of CBM shifts from G point to the middle of the G–M path (Figure S3), resulting in only a slight shift in the energy position of CBM. The above results reveal that the band gaps of 2D α- and β-Sb_2TeSe_2 can be flexibly modulated by applying an external strain, which would endow them with a wider range of applications in electronics and optoelectronics.

Carrier mobility plays a key role in determining the photoelectric conversion efficiency of 2D materials. Therefore, we estimated the carrier mobility of the α- and β-Sb_2TeSe_2 monolayers on the basis of the deformation potential (DP) theory.[36] According to the DP theory, the carrier mobility (μ) of a 2D material can be expressed as

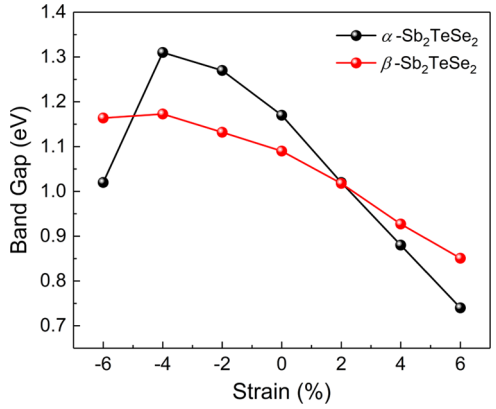

Figure 4. Band gap variation of the α- and β-Sb_2TeSe_2 monolayers as a function of external biaxial strain.

$$\mu_{2D} = \frac{e\hbar^3 C_{2D}}{k_B T m_i^* m_d E_i^2} \quad (1)$$

where m_i^* is the effective mass in the transport direction and $m_d = \sqrt{m_x^* m_y^*}$ is the average effective mass. The term E_i represents the DP constant denoting the shift of CBM for

https://doi.org/10.1021/acsomega.1c02746
ACS Omega 2021, 6, 20590−20597

Table 1. Effective Mass m_i^*/m_0, Elastic Constant C (J m^{-2}), DP Constant E_i (eV), and Carrier Mobility μ (cm^2 V^{-1} s^{-1}) along the Armchair (a) and Zigzag (z) Directions for Electrons and Holes in the α- and β-Sb_2TeSe_2 Monolayers at 300 K

	carrier type	m_a^*/m_0	m_z^*/m_0	C_a	C_z	E_a	E_z	μ_a	μ_z
α-Sb_2Te_2Se	e	0.102	0.102	64.31	63.99	−6.15	−6.05	3451	3551
	h	1.256	0.434	64.31	63.99	−3.16	−4.43	147	215
β-Sb_2TeSe_2	e	0.113	0.114	69.00	68.46	−6.37	−6.40	2806	2732
	h	0.619	0.213	69.00	68.46	−4.11	−4.98	383	756

electron or VBM for hole induced by the tiny strain. C_{2D} is the elastic modulus, k_B is the Boltzmann constant, and T is the temperature (300 K). We also utilized a rectangle supercell for the α- and β-Sb_2TeSe_2 monolayers to give an intuitive demonstration of carrier conduction along different directions (Figure S4). All of the quantities were calculated at the HSE06 level of theory.

As summarized in Table 1, the electron mobility of the α- and β-Sb_2TeSe_2 monolayers are much higher than those of the hole, which could be attributed to the relatively small effective mass of the electron. The distinct difference between the electron and hole mobilities significantly reduces the probability of the recombination of photogenerated carriers, which is favorable for the photovoltaic performance of 2D α- and β-Sb_2TeSe_2. Remarkably, the maximum carrier mobility of the α- and β-Sb_2TeSe_2 monolayers can reach 3551 and 2806 cm^2 V^{-1} s^{-1}, respectively, which are comparable to or even higher than those of many other 2D materials such as MoS_2 (~200 cm^2 V^{-1} s^{-1}),[37] phosphorene (80−1140 cm^2 V^{-1} s^{-1}),[38] and $MnPSe_3$ (~630 cm^2 V^{-1} s^{-1}).[39] The above results reveal that the α- and β-Sb_2TeSe_2 monolayers would be promising donor materials for 2D heterojunction XSCs.

Optical Properties of the Sb_2TeSe_2 Monolayers. An effective photovoltaic material should adequately capture the sunlight, especially infrared and visible light. Thus, we computed the optical absorbance of the α- and β-Sb_2TeSe_2 monolayers to give an intuitive analysis of their light-harvesting ability. It is known that the optical properties of 2D materials are dominated by the electron−hole interaction; however, such an exciton effect is out of the framework of ordinary DFT methods. Therefore, in this work, we computed the optical absorbance of the α- and β-Sb_2TeSe_2 monolayers using the GW + BSE (Bethe−Salpeter equation) method,[40,41] which includes the electron−hole interaction. According to our computations, the quasi-particle band gap and exciton binding energy of α-Sb_2TeSe_2 (β-Sb_2TeSe_2) are 1.24 (1.18) and 0.34 (0.69) eV, respectively. As shown in Figure 5, the absorption coefficients of the α- and β-Sb_2TeSe_2 monolayers are high enough for optical absorption compared with the incident AM1.5G solar spectrum[42] and higher than those of many other 2D materials (e.g., InSe,[43] WS_2,[44] Bi_2WO_6[45]) even by an order of magnitude. Especially, the α/β-Sb_2TeSe_2 monolayers can absorb almost the entire incident solar spectrum, enabling the effective utilization of solar energy. The excellent light-harvesting ability of the α- and β-Sb_2TeSe_2 monolayers render them ideal solar-absorbing materials for XSCs.

PCE for XSCs. Since the α- and β-Sb_2TeSe_2 monolayers have suitable band gaps as well as desirable optical properties, it could be expected that the 2D XSCs based on the α- and β-Sb_2TeSe_2 monolayers would have a rather high PCE. After a systematic screening, 1T-$HfSe_2$ and BiOI monolayers were chosen as acceptor materials to construct heterojunction XSCs with α- and β-Sb_2TeSe_2 monolayers, respectively. The lattice mismatches of α-Sb_2TeSe_2/$HfSe_2$ and β-Sb_2TeSe_2/BiOI heterojunctions are 1 and 4%, respectively. The interlayer binding energies of α-Sb_2TeSe_2/$HfSe_2$ and β-Sb_2TeSe_2/BiOI are −15.63 and −20.32 meV Å^{-2}, respectively. The small lattice mismatch and considerable interlayer binding energy indicate the high feasibility of constructing these two heterojunctions.

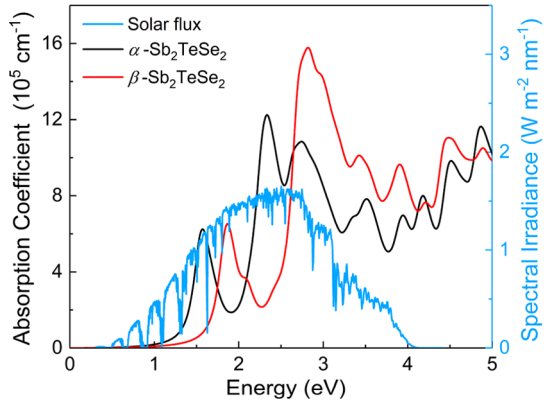

Figure 5. Absorption coefficients of the α- and β-Sb_2TeSe_2 monolayers using the GW + BSE method compared with the incident AM1.5G solar flux.

Figure 6b shows the positions of CBM and VBM of these four monolayers. Encouragingly, the conduction band offset of these two heterojunctions is within 0.20 eV, implying a high PCE. The band structure of the α-Sb_2TeSe_2/$HfSe_2$ heterojunction presented in Figure S5 shows that the VBM and CBM states are located at the Se atoms of the α-Sb_2TeSe_2 monolayer and the Hf atoms of the $HfSe_2$ monolayer, respectively. For the β-Sb_2TeSe_2/BiOI heterojunction (Figure S5), the VBM and CBM states are, respectively, located at the Se atoms of the β-Sb_2TeSe_2 monolayer and the Bi atoms of the BiOI monolayer. The detached location of VBM and CBM can facilitate the separation of electron and hole pairs in the heterojunctions.

To estimate the efficiency of 2D XSC, we referred to the method developed by Bernardi and Scharber[46] to estimate the efficiency of 2D XSCs.[10−12] The theoretical maximum PCE (η) of XSCs can be described as

$$\eta = \frac{\beta_{FF} J_{SC} V_{OC}}{P_{solar}} \quad (2)$$

where β_{FF} is the electrical fill factor with the value of 0.65, J_{SC} is the short-circuit current, which is an integral in the limit external quantum efficiency of 100% as described in eq 3, V_{OC} is an estimation of the maximum open-circuit voltage calculated by eq 4, and P_{solar} denotes the incident solar radiation, which can be obtained by integrating the AM1.5 solar energy flux according to eq 5

$$J_{SC} = \int_{E_g^d}^{\infty} \frac{P(\hbar\omega)}{\hbar\omega} d(\hbar\omega) \quad (3)$$

https://doi.org/10.1021/acsomega.1c02746
ACS Omega 2021, 6, 20590−20597

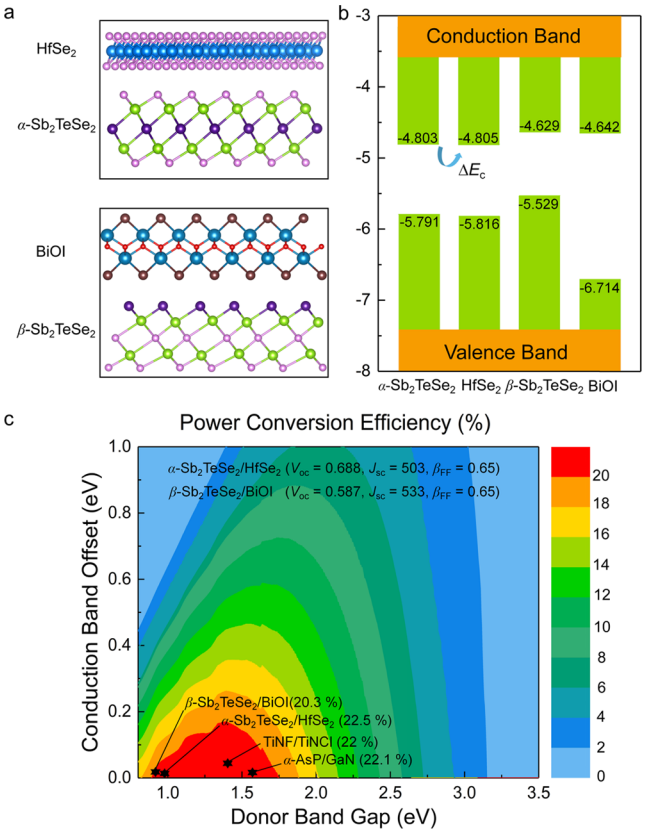

Figure 6. (a) Schematic diagrams of α-Sb_2TeSe_2/$HfSe_2$ and β-Sb_2TeSe_2/BiOI heterojunction XSCs. (b) Band alignments of α-Sb_2TeSe_2, $HfSe_2$, β-Sb_2TeSe_2, and BiOI monolayers at the HSE06+SOC level. The values of VBM and CBM are set with respect to the absolute vacuum level. (c) Computed power conversion efficiency contour as a function of the donor band gap and the conduction band offset.

$$V_{OC} = (E_g^d \Delta E_c 0.3) \quad (4)$$

$$P_{solar} = \int_0^\infty P(\hbar\omega) d(\hbar\omega) \quad (5)$$

Here, $P(\hbar\omega)$ is the AM1.5 solar energy flux (W m^{-2} eV^{-1}) at the photon energy $\hbar\omega$, E_g^d is the band gap of the donor material, ΔE_c is the conduction band offset between the donor and the acceptor materials, and the standard AM1.5 incident solar radiation P_{solar} is usually set to be 1000 W m^{-2}.[47]

Figure 6c depicts the variation in PCE as a function of the donor band gap and the conduction band offset. Remarkably, α-Sb_2TeSe_2/$HfSe_2$ and β-Sb_2TeSe_2/BiOI heterojunctions have ultrahigh PCE values of 22.5 and 20.3%, respectively, which are much larger than the highest efficiencies of OSCs (GCl-processed PM6:Y6 blend films, 17.3%),[48] ternary polymer solar cells (PM6:PDHP-Th:Y6 ternary PSCs, 16.8%),[49] and DSSCs (R6-based DSSCs, 12.6%).[50] Moreover, the computed PCE of the 2D α-Sb_2TeSe_2/$HfSe_2$ is higher than the efficiencies of the recently reported highly efficient 2D heterojunction solar cells such as MoS_2/BP (I) (20.42%),[51] $HfTeSe_4$/Bi_2WO_6 (20.8%),[29] AC-stacked green-P/$MoSe_2$ (21%),[52] α-AsP/GaN (22.1%),[53] and TiNF/TiNCl (22%).[54] The above results indicate that 2D α-Sb_2TeSe_2/$HfSe_2$ and β-Sb_2TeSe_2/BiOI heterojunctions are promising candidates for highly efficient 2D XSCs.

CONCLUSIONS

In summary, based on comprehensive DFT calculations, we systematically studied the structural, electronic, and optical properties of two novel 2D semiconducting materials, namely, the α- and β-Sb_2TeSe_2 monolayers. According to our calculations, these two monolayers are dynamically, thermally, mechanically, and chemically stable and could be experimentally synthesized via exfoliation techniques by overcoming small cleavage energy. The α- and β-Sb_2TeSe_2 monolayers have moderate band gaps (~1.1 eV) to absorb light in the whole range of the solar spectrum and show high carrier mobility up to 3000 cm^2 V^{-1} s^{-1}. The moderate band gaps of the α- and β-Sb_2TeSe_2 monolayers make them suitable donor materials to construct 2D heterojunction XSCs. As a result, the designed α-Sb_2TeSe_2/$HfSe_2$ and β-Sb_2TeSe_2/BiOI heterojunction XSCs show high PCEs of up to 22.5 and 20.3%, respectively, rendering them appealing candidates for photovoltaics.

ASSOCIATED CONTENT

Supporting Information

The Supporting Information is available free of charge at https://pubs.acs.org/doi/10.1021/acsomega.1c02746.

Snapshots of the equilibrium structures of the Sb_2TeSe_2 monolayers at 600 K at the end of 10 ps FPMD simulations, band edge position variations under strain, electronic band structure of the α-Sb_2TeSe_2 monolayer at a compression strain of −6%, orthogonal supercells of the Sb_2TeSe_2 monolayers, and stacking patterns and band structures of the α-Sb_2TeSe_2/$HfSe_2$ and β-Sb_2TeSe_2/BiOI heterojunctions (PDF)

AUTHOR INFORMATION

Corresponding Authors

Xiaocheng Zhou − *Jiangsu Key Laboratory of New Power Batteries, Jiangsu Collaborative Innovation Centre of Biomedical Functional Materials, School of Chemistry and Materials Science, Nanjing Normal University, Nanjing 210023, China*; Email: xczhou@njnu.edu.cn

Ya-fei Li − *Jiangsu Key Laboratory of New Power Batteries, Jiangsu Collaborative Innovation Centre of Biomedical Functional Materials, School of Chemistry and Materials Science, Nanjing Normal University, Nanjing 210023, China*; orcid.org/0000-0003-2587-820X; Email: liyafei@njnu.edu.cn

Authors

Chun Wang − *Jiangsu Key Laboratory of New Power Batteries, Jiangsu Collaborative Innovation Centre of Biomedical Functional Materials, School of Chemistry and Materials Science, Nanjing Normal University, Nanjing 210023, China*

Yu Jing − *Jiangsu Co-Innovation Centre of Efficient Processing and Utilization of Forest Resources, College of Chemical Engineering, Nanjing Forestry University, Nanjing 210037, China*; orcid.org/0000-0002-1537-9522

Complete contact information is available at: https://pubs.acs.org/10.1021/acsomega.1c02746

Notes

The authors declare no competing financial interest.

https://doi.org/10.1021/acsomega.1c02746
ACS Omega 2021, 6, 20590−20597

■ ACKNOWLEDGMENTS

We are grateful for funding support from the National Key R&D Program of China (2019YFA0308000), the Natural Science Foundation of China (Nos. 21873050 and 21903046), and NSF of Jiangsu Province of China (No. BK20190744). The computational resources utilized in this research were provided by Shanghai Supercomputer Centre.

■ REFERENCES

(1) Chapin, D. M.; Fuller, C. S.; Pearson, G. L. A New Silicon P-N Junction Photocell for Converting Solar Radiation into Electrical Power. *J. Appl. Phys.* **1954**, *25*, 676−677.
(2) Battaglia, C.; Cuevas, A.; de Wolf, S. High-Efficiency Crystalline Silicon Solar Cells: Status and Perspectives. *Energy Environ. Sci.* **2016**, *9*, 1552−1576.
(3) Bauhuis, G. J.; Mulder, P.; Haverkamp, E. J.; Huijben, J. C. C. M.; Schermer, J. J. 26.1% Thin-Film GaAs Solar Cell Using Epitaxial Lift-Off. *Sol. Energy Mater. Sol. Cells* **2009**, *93*, 1488−1491.
(4) Wu, X. High-Efficiency Polycrystalline CdTe Thin-Film Solar Cells. *Sol. Energy* **2004**, *77*, 803−814.
(5) Zhao, W. C.; Li, S. S.; Yao, H. F.; Zhang, S. Q.; Zhang, Y.; Yang, B.; Hou, J. H. Molecular Optimization Enables over 13% Efficiency in Organic Solar Cells. *J. Am. Chem. Soc.* **2017**, *139*, 7148−7151.
(6) Gong, J.; Sumathy, K.; Qiao, Q.; Zhou, Z. Review on Dye-Sensitized Solar Cells (DSSCs): Advanced Techniques and Research Trends. *Renewable Sustainable Energy Rev.* **2017**, *68*, 234−246.
(7) Wu, K.; Ma, H.; Gao, Y.; Hu, W.; Yang, J. Highly-Efficient Heterojunction Solar Cells Based on Two-Dimensional Tellurene and Transition Metal Dichalcogenides. *J. Mater. Chem. A* **2019**, *7*, 7430−7436.
(8) Linghu, J.; Yang, T.; Luo, Y.; Yang, M.; Zhou, J.; Shen, L.; Feng, Y. P. High-Throughput Computational Screening of Vertical 2D van Der Waals Heterostructures for High-Efficiency Excitonic Solar Cells. *ACS Appl. Mater. Interfaces* **2018**, *10*, 32142−32150.
(9) Cai, Z.; Liu, B.; Zou, X.; Cheng, H.-M. Chemical Vapor Deposition Growth and Applications of Two-Dimensional Materials and Their Heterostructures. *Chem. Rev.* **2018**, *118*, 6091−6133.
(10) Ganesan, V. D. S. O.; Linghu, J.; Zhang, C.; Feng, Y. P.; Shen, L. Heterostructures of Phosphorene and Transition Metal Dichalcogenides for Excitonic Solar Cells: A First-Principles Study. *Appl. Phys. Lett.* **2016**, *108*, No. 122105.
(11) Guo, H.; Lu, N.; Dai, J.; Wu, X.; Zeng, X. C. Phosphorene Nanoribbons, Phosphorus Nanotubes, and van der Waals Multilayers. *J. Phys. Chem. C* **2014**, *118*, 14051−14059.
(12) Rawat, A.; Ahammed, R.; Dimple; Jena, N.; Mohanta, M. K.; De Sarkar, A. Solar Energy Harvesting in Type II van Der Waals Heterostructures of Semiconducting Group III Monochalcogenide Monolayers. *J. Phys. Chem. C* **2019**, *123*, 12666−12675.
(13) Li, B.; Zhai, R.; Fang, T.; Xia, K.; Wu, Y.; Zhu, T. Mid-Temperature Thermoelectric Performance of Zone-Melted $Sb_2(Te, Se)_3$ Alloys near Phase Transition Boundary. *J. Materiomics* **2019**, *5*, 590−596.
(14) Eremeev, S. V.; Vergniory, M. G.; Menshchikova, T. V.; Shaposhnikov, A. A.; Chulkov, E. V. The Effect of van der Waal's Gap Expansions on the Surface Electronic Structure of Layered Topological Insulators. *New J. Phys.* **2012**, *14*, No. 113030.
(15) Lee, C. K.; Cheng, C. M.; Weng, S. C.; Chen, W. C.; Tsuei, K. D.; Yu, S. H.; Chou, M. M.; Chang, C. W.; Tu, L. W.; Yang, H. D.; Luo, C. W.; Gospodinov, M. M. Robustness of a Topologically Protected Surface State in a Sb_2Te_2Se Single Crystal. *Sci. Rep.* **2016**, *6*, No. 36538.
(16) Kresse, G.; Hafner, J. Ab Initio Molecular Dynamics for Liquid Metals. *Phys. Rev. B: Condens. Matter Mater. Phys.* **1993**, *47*, 558−561.
(17) Blöchl, P. E. Projector Augmented-Wave Method. *Phys. Rev. B: Condens. Matter Mater. Phys.* **1994**, *50*, No. 17953.
(18) Kresse, G.; Joubert, D. From Ultrasoft Pseudopotentials to the Projector Augmented-Wave Method. *Phys. Rev. B: Condens. Matter Mater. Phys.* **1999**, *59*, 1758−1775.
(19) Perdew, J. P.; Burke, K.; Ernzerhof, M. Generalized Gradient Approximation Made Simple. *Phys. Rev. Lett.* **1996**, *77*, No. 3865.
(20) Heyd, J.; Scuseria, G. E.; Ernzerhof, M. Hybrid Functionals Based on a Screened Coulomb Potential. *J. Chem. Phys.* **2003**, *118*, 8207−8215.
(21) Turro, N. J.; Kavarnos, G.; Fung, V.; Lyons, A. L.; Cole, T. A Spectroscopic Study of Some Dibromonaphthonorbornenes. Possible Case of Inverse External Heavy Atom Induced Spin Orbital Coupling. *J. Am. Chem. Soc* **1972**, *94*, 1392−1394.
(22) Grimme, S. Semiempirical GGA-Type Density Functional Constructed with a Long-Range Dispersion Correction. *J. Comput. Chem.* **2006**, *27*, 1787−1799.
(23) Baroni, S.; de Gironcoli, S.; Dal Corso, A.; Giannozzi, P. Phonons and Related Crystal Properties from Density-Functional Perturbation Theory. *Rev. Mod. Phys.* **2001**, *73*, 515−562.
(24) Togo, A.; Oba, F.; Tanaka, I. First-Principles Calculations of the Ferroelastic Transition Between Rutile-Type and $CaCl_2$-Type SiO_2 at High Pressures. *Phys. Rev. B: Condens. Matter Mater. Phys.* **2008**, *78*, No. 134106.
(25) Nosé, S. A Unified Formulation of the Constant Temperature Molecular Dynamics Method. *J. Chem. Phys.* **1984**, *81*, 511−519.
(26) Martyna, G. J.; Klein, M. L.; Tuckerman, M. Nosé-Hoover Chains: The Canonical Ensemble via Continuous Dynamics. *J. Chem. Phys.* **1992**, *97*, 2635−2643.
(27) Mounet, N.; Gibertini, M.; Schwaller, P.; Campi, D.; Merkys, A.; Marrazzo, A.; Sohier, T.; Castelli, I. E.; Cepellotti, A.; Pizzi, G.; Marzari, N. Two-Dimensional Materials from High-Throughput Computational Exfoliation of Experimentally Known Compounds. *Nat. Nanotechnol.* **2018**, *13*, 246−252.
(28) Mak, K. F.; Lee, C.; Hone, J.; Shan, J.; Heinz, T. F. Atomically Thin MoS_2: A New Direct-Gap Semiconductor. *Phys. Rev. Lett.* **2010**, *105*, No. 136805.
(29) Yang, H.; Ma, Y.; Liang, Y.; Huang, B.; Dai, Y. Monolayer $HfTeSe_4$: A Promising Two-Dimensional Photovoltaic Material for Solar Cells with High Efficiency. *ACS Appl. Mater. Interfaces* **2019**, *11*, 37901−37907.
(30) Dai, J.; Zeng, X. C. Titanium Trisulfide Monolayer: Theoretical Prediction of a New Direct-Gap Semiconductor with High and Anisotropic Carrier Mobility. *Angew. Chem., Int. Ed.* **2015**, *54*, 7572−7576.
(31) Zacharia, R.; Ulbricht, H.; Hertel, T. Interlayer Cohesive Energy of Graphite from Thermal Desorption of Polyaromatic Hydrocarbons. *Phys. Rev. B: Condens. Matter Mater. Phys.* **2004**, *69*, No. 155406.
(32) Björkman, T.; Gulans, A.; Krasheninnikov, A. V.; Nieminen, R. M. Van Der Waals Bonding in Layered Compounds from Advanced Density-Functional First-Principles Calculations. *Phys. Rev. Lett.* **2012**, *108*, No. 235502.
(33) Mouhat, F.; Coudert, F.-X. Necessary and Sufficient Elastic Stability Conditions in Various Crystal Systems. *Phys. Rev. B* **2014**, *90*, No. 224104.
(34) Ju, L.; Shang, J.; Tang, X.; Kou, L. Tunable Photocatalytic Water Splitting by the Ferroelectric Switch in a 2D $AgBiP_2Se_6$ Monolayer. *J. Am. Chem. Soc.* **2020**, *142*, 1492−1500.
(35) Qiao, M.; Chen, Y.; Wang, Y.; Li, Y. The Germanium Telluride Monolayer: A Two Dimensional Semiconductor with High Carrier Mobility for Photocatalytic Water Splitting. *J. Mater. Chem. A* **2018**, *6*, 4119−4125.
(36) Bardeen, J.; Shockley, W. Deformation Potentials and Mobilities in Non-Polar Crystals. *Phys. Rev.* **1950**, *80*, No. 72.
(37) Cai, Y.; Zhang, G.; Zhang, Y.-W. Polarity-Reversed Robust Carrier Mobility in Monolayer MoS_2 Nanoribbons. *J. Am. Chem. Soc.* **2014**, *136*, 6269−6275.
(38) Qiao, J.; Kong, X.; Hu, Z.-X.; Yang, F.; Ji, W. High-Mobility Transport Anisotropy and Linear Dichroism in Few-Layer Black Phosphorus. *Nat. Commun.* **2014**, *5*, No. 4475.
(39) Zhang, X.; Zhao, X.; Wu, D.; Jing, Y.; Zhou, Z. $MnPSe_3$ Monolayer: A Promising 2D Visible-Light Photohydrolytic Catalyst with High Carrier Mobility. *Adv. Sci.* **2016**, *3*, No. 1600062.

https://doi.org/10.1021/acsomega.1c02746
ACS Omega 2021, 6, 20590−20597

(40) Rohlfing, M.; Louie, S. G. Electron-Hole Excitations and Optical Spectra from First Principles. *Phys. Rev. B: Condens. Matter Mater. Phys.* **2000**, *62*, 4927−4944.
(41) Onida, G.; Reining, L.; Rubio, A. Electronic Excitations: Density-Functional Versus Many-Body Green's-Function Approaches. *Rev. Mod. Phys.* **2002**, *74*, 601−659.
(42) Gueymard, C. A. The Sun's Total and Spectral Irradiance for Solar Energy Applications and Solar Radiation Models. *Sol. Energy* **2004**, *76*, 423−453.
(43) Li, Z.; Qiao, H.; Guo, Z.; Ren, X.; Huang, Z.; Qi, X.; Dhanabalan, S. C.; Ponraj, J. S.; Zhang, D.; Li, J.; Zhao, J.; Zhong, J.; Zhang, H. High-Performance Photo-Electrochemical Photodetector Based on Liquid-Exfoliated Few-Layered InSe Nanosheets with Enhanced Stability. *Adv. Funct. Mater.* **2018**, *28*, No. 1705237.
(44) Cong, C.; Shang, J.; Wang, Y.; Yu, T. Optical Properties of 2D Semiconductor WS_2. *Adv. Opt. Mater.* **2018**, *6*, No. 1700767.
(45) Zhou, Y.; Zhang, Y.; Lin, M.; Long, J.; Zhang, Z.; Lin, H.; Wu, J. C.; Wang, X. Monolayered Bi_2WO_6 Nanosheets Mimicking Heterojunction Interface with Open Surfaces for Photocatalysis. *Nat. Commun.* **2015**, *6*, No. 8340.
(46) Scharber, M. C.; Mühlbacher, D.; Koppe, M.; Denk, P.; Waldauf, C.; Heeger, A. J.; Brabec, C. J. Design Rules for Donors in Bulk-Heterojunction Solar Cells-Towards 10% Energy-Conversion Efficiency. *Adv. Mater.* **2006**, *18*, 789−794.
(47) Servaites, J. D.; Ratner, M. A.; Marks, T. J. Practical Efficiency Limits in Organic Photovoltaic Cells: Functional Dependence of Fill Factor and External Quantum Efficiency. *Appl. Phys. Lett.* **2009**, *95*, No. 163302.
(48) Liu, L.; Kan, Y.; Gao, K.; Wang, J.; Zhao, M.; Chen, H.; Zhao, C.; Jiu, T.; Jen, A.-K.-Y.; Li, Y. Graphdiyne Derivative as Multifunctional Solid Additive in Binary Organic Solar Cells with 17.3% Efficiency and High Reproductivity. *Adv. Mater.* **2020**, *32*, No. 1907604.
(49) Han, J.; Wang, X.; Huang, D.; Yang, C.; Yang, R.; Bao, X. Employing Asymmetrical Thieno[3,4-d]pyridazin-1(2*H*)-one Block Enables Efficient Ternary Polymer Solar Cells with Improved Light-Harvesting and Morphological Properties. *Macromolecules* **2020**, *53*, 6619−6629.
(50) Ren, Y.; Sun, D.; Cao, Y.; Tsao, H. N.; Yuan, Y.; Zakeeruddin, S. M.; Wang, P.; Grätzel, M. A Stable Blue Photosensitizer for Color Palette of Dye-Sensitized Solar Cells Reaching 12.6% Efficiency. *J. Am. Chem. Soc.* **2018**, *140*, 2405−2408.
(51) Mohanta, M. K.; Rawat, A.; Jena, N.; Dimple; Ahammed, R.; De Sarkar, A. Interfacing Boron Monophosphide with Molybdenum Disulfide for an Ultrahigh Performance in Thermoelectrics, Two-Dimensional Excitonic Solar Cells, and Nanopiezotronics. *ACS Appl. Mater. Interfaces* **2020**, *12*, 3114−3126.
(52) Kaur, S.; Kumar, A.; Srivastava, S.; Tankeshwar, K.; Pandey, R. Monolayer, Bilayer, and Heterostructures of Green Phosphorene for Water Splitting and Photovoltaics. *J. Phys. Chem. C* **2018**, *122*, 26032−26038.
(53) Xie, M.; Zhang, S.; Cai, B.; Huang, Y.; Zou, Y.; Guo, B.; Gu, Y.; Zeng, H. A Promising Two-Dimensional Solar Cell Donor: Black Arsenic-Phosphorus Monolayer with 1.54 eV Direct Bandgap and Mobility Exceeding 14,000 $cm^2 V^{-1} S^{-1}$. *Nano Energy* **2016**, *28*, 433−439.
(54) Liang, Y.; Dai, Y.; Ma, Y.; Ju, L.; Wei, W.; Huang, B. Novel Titanium Nitride Halide TiNX (X = F, Cl, Br) Monolayers: Potential Materials for Highly Efficient Excitonic Solar Cells. *J. Mater. Chem. A* **2018**, *6*, 2073−2080.

https://doi.org/10.1021/acsomega.1c02746
ACS Omega 2021, 6, 20590−20597